Single Wall Carbon Nanotube Supports for Portable Direct Methanol Fuel Cells

G. Girishkumar,[†] Timothy D. Hall,[‡] K. Vinodgopal,*[,†,§] and Prashant V. Kamat*[,†,‡]

Radiation Laboratory and Departments of Chemistry & Biochemistry and Chemical & Biomolecular Engineering, University of Notre Dame, Notre Dame, Indiana 46556-0579, and Department of Chemistry, Indiana University Northwest, Gary, Indiana 46408

Received: August 23, 2005; In Final Form: October 10, 2005

Single-wall and multiwall carbon nanotubes are employed as carbon supports in direct methanol fuel cells (DMFC). The morphology and electrochemical activity of single-wall and multiwall carbon nanotubes obtained from different sources have been examined to probe the influence of carbon support on the overall performance of DMFC. The improved activity of the Pt−Ru catalyst dispersed on carbon nanotubes toward methanol oxidation is reflected as a shift in the onset potential and a lower charge transfer resistance at the electrode/electrolyte interface. The evaluation of carbon supports in a passive air breathing DMFC indicates that the observed power density depends on the nature and source of carbon nanostructures. The intrinsic property of the nanotubes, dispersion of the electrocatalyst and the electrochemically active surface area collectively influence the performance of the membrane electrode assembly (MEA). As compared to the commercial carbon black support, single wall carbon nanotubes when employed as the support for anchoring the electrocatalyst particles in the anode and cathode sides of MEA exhibited a ∼30% enhancement in the power density of a single stack DMFC operating at 70 °C.

Introduction

It is anticipated that soon, fuel cells based on liquid feeds such as methanol will replace batteries in low power electronic applications such as cell phones and laptop computers.[1,2] Direct methanol fuel cells (DMFC) appear to be the most promising, although significant improvements in performance and design are still necessary before use.[3] Performance related issues include methanol crossover through the Nafion membrane, catalyst performance and sluggish kinetics at both anode and cathode, and the effect of corrosion of the carbon support in acidic environment.[4,5] Cost considerations entail reducing the amount of precious metal catalyst without sacrificing power output. A key consideration in achieving such a gain is the nature of the carbon support, which can assist both in dispersion of the metal catalyst and in possibly facilitating electron and mass transfer kinetics at the electrode interface. A variety of carbon supports have been investigated in this direction including graphite nanofibers, single walled carbon nanotubes (SWCNTs), multiwalled carbon nanotubes (MWCNTs), and high surface area carbon blacks.[6−9]

The graphitic carbon nanofibers (GNF) with average diameters between 150 and 200 nm are substantially wider than either the single or multiwall carbon nanotubes. Nevertheless, several groups have used these GNF supports with metal catalyst as electrodes for DMFC applications.[10,11] The morphology, electronic and mechanical properties of carbon nanotubes make them particularly attractive candidates for surmounting some of the above-mentioned technical problems such as sluggish electrode kinetics and surface area limitations. The microporous nature and high surface area of the carbon nanotubes should facilitate better transport of both oxidant and fuel and much higher catalyst utilization than conventional supports such as carbon blacks.[12−14] In a recent paper, we reported the oxidation of methanol at platinum catalyst dispersed on SWCNT films that had been electrophoretically deposited on optically transparent electrodes.[15] This study based on cyclic voltammetry showed that single walled carbon nanotubes are useful as carbon supports for fuel cell applications such as methanol oxidation and oxygen reduction. A number of different groups have attempted to employ MWCNTs as catalyst support in DMFC with the particular emphasis on elucidating the role of carbon nanotubes in facilitating oxygen reduction.[16,17] The use of nanotubes as a carbon support for fuel cell applications is yet to be explored fully.

Additionally, systematic comparisons of data obtained by using different carbon nanotube supports, e.g., SWCNTs and MWCNTs, in direct methanol fuel cells are unavailable. Factors such as available surface area, conductivity, porosity of support, and utilization of catalyst contribute to the overall performance of a DMFC. The single wall carbon nanotubes themselves often have quite different properties depending upon the chirality. Thus, SWCNTs can be metallic or semiconducting in nature, and a given sample can have a wide distribution of tube diameters. This in turn can influence the electrocatalytic properties, such as interfacial impedance and charge-transfer kinetics. In principle, SWCNTs are seamless cylinders, but they often have defect sites, where the attachment of platinum or platinum−ruthenium catalyst particles is most likely to occur. The density of defect sites and differences thereof between different sources of SWCNT can play an important role in determining the performance of a DMFC.

The ability therefore to navigate this complex welter of data on carbon nanotubes and other carbon nanosupports and yet be able to have a working DMFC based on carbon nanotube

* To whom correspondence should be addressed. E-mail: pkamat@nd.edu. Tel.: 574-631-5411. Fax: 574-631-8068.

[†] Radiation Laboratory, University of Notre Dame.

[‡] Departments of Chemistry & Biochemistry and Chemical & Biomolecular Engineering, University of Notre Dame.

[§] Indiana University Northwest.

10.1021/jp054764i CCC: $33.50
Published on Web 11/17/2005

electrodes with optimal properties can be quite challenging. We report here a systematic effort to probe the electrochemistry of methanol oxidation using a variety of nanotube supports, both single and multiwall, with the intent to optimize the performance of these supports in a DMFC.

Experimental Section

Purified SWCNT samples were obtained from three different sources: Nanocs, Inc. (New York), Bucky USA (Houston), and SES Research (Houston). MWCNTs were obtained from Nanostructured & Amorphous Materials Inc. (Houston). Carbon black was obtained from Johnson Matthey (London, UK). The pristine nanotubes were used as is with no further chemical treatment.

Deposition of CNT and Platinum−Ruthenium on Carbon Fiber Electrode (CFE). To ensure proper contact with the carbon support and the Pt−Ru, a single-pot procedure was used for the preparation of the electrodes. We employed 2.25 × 2.25 cm^2 electrodes cut from carbon fiber paper (0.6 mm thickness) obtained from Fuel Cell Store (Boulder, CO). For the preparation of the catalyst ink, 20 mg of the nanotubes or another carbon support was mixed with 10 mL of 2-propanol. 80 mg of a 5% Nafion solution (Aldrich) was added to this mixture, which was then sonicated for 1 h so that the nanotubes were completely suspended in the solvent. 10 mg of Pt−Ru catalyst from Johnson Matthey was mixed with the nanotube solution and sonicated for 30 min. The suspension was further stirred overnight. At the end of the process, the catalyst and the carbon support were completely mixed. The solution thus obtained was brushed on to the carbon fiber paper electrode (CFE) and then dried. If necessary, the process of deposition, drying, and weighing was continued until the desired loading (±0.05 mg/cm^2) of the catalyst was obtained.

Characterization of the Electrode Surface. The carbon fiber electrodes containing SWCNT and Pt−Ru were characterized by Raman spectroscopy using a JASCO Ventuno Raman spectrometer. The laser power used was 10 mW. A radiation spot of 0.1 mm diameter was used in 180 degree backscattering geometry at room temperature. The excitation wavelength was 532 nm. The morphology of the carbon fiber electrode deposited with SWCNT, carbon black and Pt−Ru were characterized by Hitachi S-4500 scanning electron microscopy (SEM).

Preparation of the Membrane Electrode Assembly (MEA) for Evaluation in Fuel Cells. The catalyst layers of anode and cathode were deposited on a carbon fiber paper (Toray) and a carbon cloth coated with Teflon, (Electrochem Inc.), respectively. The preparation of the individual electrodes is described elsewhere.[18] Nafion 117 membrane (DuPont) was pretreated by immersion in boiling solution of 3 vol % H_2O_2 (1 hr) and 1 M H_2SO_4 (1 hr), followed by cleaning in distilled water. The membrane was stored in distilled water before use. The catalyzed electrodes for the anode and cathode respectively were positioned on both sides of the pretreated Nafion 117 and hot pressed at 120 °C and 50 kg cm^{-2} for 2 min to form a unit of MEA.

Electrochemical Characterization. Half-cell reactions were conducted in a three-arm electrochemical cell using the carbon fiber paper coated with SWCNTs and Pt black as an anode or cathode. Cyclic voltammetric experiments were carried out using BAS 100 electrochemical analyzer.

The impedance spectra were recorded using a Gamry DC 101 frequency response analyzer, in the frequency range between 100 kHz and 100 MHz and an excitation signal of 10 mV (rms). The experiment was conducted in a potentiostatic EIS mode where we were able to record the impedance spectra at open circuit potential or at controlled overpotentials. The electrolyte (1 M H_2SO_4 solution) was purged with nitrogen for 30 min. The surface of the working electrode was refreshed by cycling the potential between −0.3 to 1.0 V vs SCE at 50 mV/s, until the voltammogram showed no changes. The electrode was then subjected to desired value of potential for carrying out the impedance measurements.

The electrochemically active surface area was measured by the CO adsorption on a carbon fiber electrode deposited with a variety of carbon supports and Pt−Ru. Extra precautions were taken with the experiments involving CO adsorption. Purging of CO was carried out in a fume hood with CO monitor attached outside the hood.

Catalyst Evaluation in a Direct Methanol Fuel Cell. Room temperature fuel cell evaluation of the different carbon supports/catalysts was carried out using a passive air breathing fuel cell purchased from Fuelcellstore.com. This fuel cell contains a reservoir that can store the methanol at the anode, and the cathode compartment is exposed to air. This assembly provides the features of operation of a stationary or passive air breathing fuel cell.

For the evaluation of the catalyst in a high-temperature fuel cell, we used a single-stack cell test fixture supplied by Scribner Associates, Inc. (North Carolina). The MEA was inserted between two graphite plates that had a serpentine flow pattern. Two silicone gaskets of thickness 0.24 mm were introduced between the membrane and electrodes. A uniform torque of 35 inch-pounds was applied to each of the bolts used to assemble the cell. The fuel cell was connected to the test station (Scribner Associates, Inc.) that was equipped with a gas humidifier, a mass flow controller, and a temperature indicator controller. The MEA was subjected to pretreatment by passing through humidified hydrogen and oxygen gases, which were fed into the cell at a flow rate of 200 cm^3 min^{-1}. The cell was maintained at a temperature of 75 °C overnight under these gas flow conditions. We have found that this procedure yields a better performance than passing water through the anode compartment. The current−voltage ($I-V$) characteristics of the cell were evaluated at two different ambient temperatures of 25 °C and 70 °C.

Results and Discussion

Methanol Oxidation Using Different Carbon Nanotubes Supports. The catalyst of choice for the anodic oxidation of methanol is platinum−ruthenium alloy.[19,20] Methanol adsorbs on the platinum surface and undergoes a sequential six-electron oxidation. The presence of the ruthenium in the catalyst alloy serves to reduce the poisoning of the Pt surface by carbon monoxide. We prepared carbon fiber electrodes (CFE) using the nanotube supports obtained from different sources and Pt−Ru catalysts as discussed in the Experimental Section. The loading of the metal alloy, Pt−Ru (0.4 mg/cm^2), carbon support (0.9 mg/cm^2), and the geometric area of the electrode were maintained constant in all cases, for comparison. The electrochemical activity of the different carbon supports was tested in a half-cell reaction using cyclic voltammetry. The voltammograms recorded by oxidizing 1 M methanol in 1 M H_2SO_4 solution are shown in Figure 1. For comparison, we have used a commercial carbon black (CB) support obtained from Johnson Matthey. Methanol oxidation is represented by the anodic peak around 600−800 mV. In the reverse scan, the adsorbed intermediates produce a second oxidation peak at ∼350 mV. The magnitude of the peak current at 800 mV is directly proportional to the amount of methanol oxidized at the electrode, and hence the activity of the electrode. The Tafel plot analysis and comparison between SWCNT and carbon support have been discussed in our earlier study.[15]

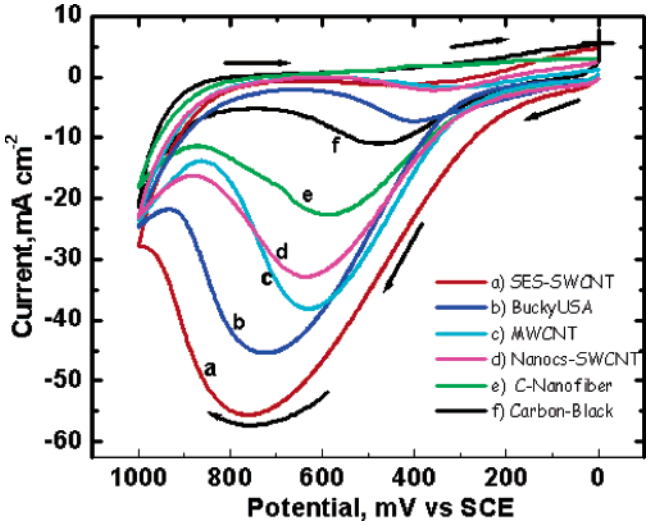

Figure 1. Cyclic voltammetric traces of methanol oxidation (1 M) in 1 M H_2SO_4 recorded using CFE/carbon support/Pt−Ru system. Each trace corresponds to a different carbon support (a) SES−SWCNT, (b) Bucky USA-SWCNT, (c) MWCNT, (d) Nanocs-SWCNT, (e) C-nanofiber, (f) carbon black. Scan rate was 20 mV/s. Platinum−ruthenium loading was 0.4 mg/cm^2 and the amount of carbon support was 0.9 mg/cm^2 in each case.

For a CFE/SES−SWCNT/Pt−Ru electrode, we observe a maximum methanol oxidation current between 50 and 60 mA/cm^2. In comparison the CFE/CB/Pt−Ru electrode yields only about 10 mA/cm^2 of current. The enhancement in the oxidation current observed with nanostructures is indicative of the important role SWCNT plays in promoting the methanol oxidation. The cyclic voltammograms show an initial activation period as the oxidation current increases with repetitive scans between 0 and 1.0 V and stabilizes after about six scans.

Another important aspect of these carbon supports is their influence on the onset potential at which methanol oxidation occurs.[21] As compared to carbon black support, the nanotube supports exhibit lower onset potentials (up to 130 mV). The onset potentials for methanol oxidation recorded using different carbon supports are compared in Table 1. The shift in the anodic potential that we observe with SWCNT is likely to arise from a change in the work function of SWCNTs ($\Phi_{CNT} \sim 5$ eV).[22,23] Such an effect complements the effect usually seen when Ru is incorporated into the electrocatalyst.[19] The observed shift in the onset potential and the enhanced anodic current at SWCNT electrode is an indication of the catalytic role that SWCNT plays during the methanol oxidation process.

Comparison of Surface Area of the Carbon Supports. It is interesting to note from Table 1 that the observed effect of carbon support on the onset potential and methanol oxidation current varies in magnitude. The question arises whether the difference in the electrochemical behavior between the various electrodes can be correlated with the physical and intrinsic properties of the carbon supports. First, we compared the surface areas of these supports. While carbon nanotubes are acknowledged to have very high surface areas, the actual numbers vary depending on the source. For example, BET surface area of SWCNTs obtained from Nanocs Inc. was 244 m^2/g, which was significantly higher than the value, 81 m^2/g, of SWCNT sample obtained from SES Inc. Because of the intertubular attraction and/or bundling effect, these samples exhibit varying degrees of adsorption of nitrogen. The obvious question is whether higher BET surface area would render higher activity for the electrocatalyst. Several studies have indicated that optimum performance of the catalyst can be obtained with a carbon support surface area of 70−80 m^2/g.[24]

Electrochemically active surface area (ECSA) measurement, on the other hand, is a better measure by which to obtain an effective electrocatalyst surface area that is accessible for the reaction at the electrochemical interface. The electrochemically active surface area (ECSA) of SWCNT-Pt−Ru was determined by the procedure described in the literature.[25] In a typical experiment, the electrode potential was cycled between 0.3 and 1.2 V vs SCE in 0.1 M H_2SO_4 solution (scan rate of 50 mV/s) until stable response was attained. The electrode was then maintained at a potential of −0.150 V vs SCE. CO was bubbled through the solution for 5 min to ensure complete coverage of the electrode surface. The dissolved CO in solution was removed by purging the solution with N_2. This step was followed by stripping of the adsorbed CO from the electrode surface by sweeping the potential from −0.1 V to 1.2 V vs SCE. The CO oxidation charge as measured from the anodic current peak was used to determine the ECSA (see Figure S1 as Supporting Information information).

It is interesting that BET surface area obtained for different carbon supports does not follow the trend of ESCA measurements (Table 1). All nanostructured carbon supports show relatively similar ECSA ~2.1−2.6 × 10^4 cm^2/gPt. These values are significantly higher than the one obtained for carbon black support (0.8 × 10^4 cm^2/g Pt). It is evident that the ability of nanotubes to disperse and anchor Pt−Ru catalyst effectively is an important factor in attaining higher ECSA. While ECSA is an important factor for determining the electrochemical activity of the Pt−Ru catalyst, it alone cannot explain the observed differences in the electrochemical performance toward methanol oxidation. The intrinsic properties of SWCNT will also be important contributing factors in delivering higher catalytic activity for the Pt−Ru catalyst.

Electrode Characterization. Another important factor for achieving a good dispersion of the Pt−Ru catalyst is the morphology of the carbon supports. SEM images taken after modification of carbon fiber electrode with SWCNT, and Pt−

TABLE 1: Variation of the Onset Potential, BET Surface Area and Effective Platinum Surface Utilization Area of the Electrode with Type of Carbon Support on Anode

electrodes Pt−Ru	surface area[a] (m^2/g)	ECSA[b] cm^2/gPt	onset potential[c] mV/SCE	methanol oxidation[d] mA/cm^2	power density[e] mW/cm^2
SES−SWCNT	81	2.5 × 10^4	170	55	4.2
BuckyUSA-SWCNT	475	1.2 × 10^4	240	45	3.6
Nanocs-SWCNT	244	2.6 × 10^4	256	37	1.1
MWCNT	377	2.1 × 10^4	262	32	2.3
carbon nanofiber	25	2.2 × 10^4	280	22	1.7
JM-carbon black	80	0.8 × 10^4	300	11	1.0

[a] BET surface area of carbon support using nitrogen adsorption isotherms. [b] Obtained from CO stripping. [c] Using Pt−Ru electrocatalyst anchored on carbon support. [d] From cyclic voltammetry. [e] Air breathing methanol cell at 25 °C.

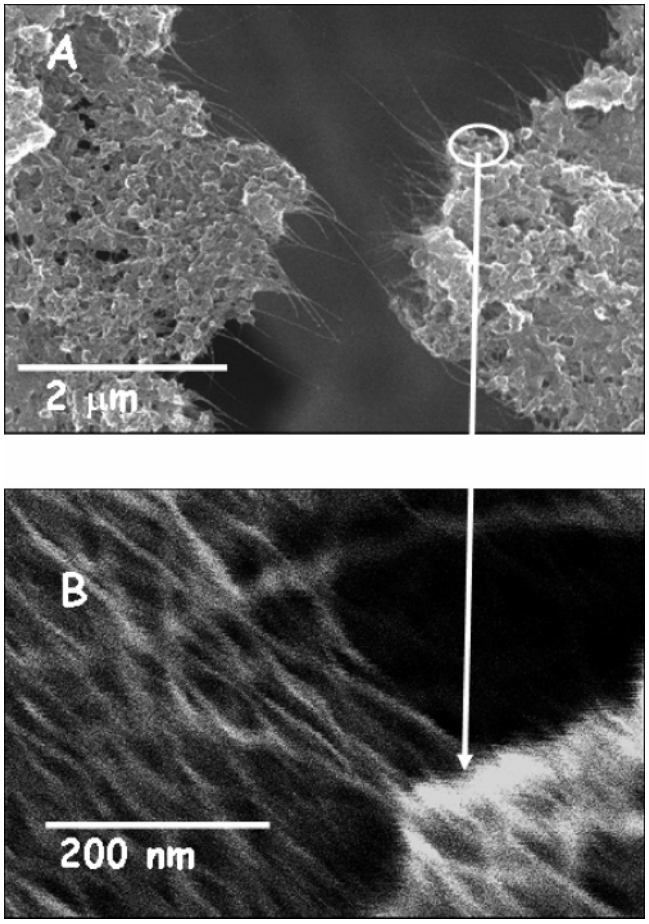

Figure 2. Scanning electron micrograph showing carbon fiber electrode (CFE) deposited with SWCNT and Pt−Ru at low magnification (A) and high magnification (B).

Ru catalyst are shown in Figure 2A (low magnification) and 2B (high magnification). As seen from the SEM, the carbon paper (Figure S2 in Supporting Information) is a network of carbon fibers. These macrofibers provide the foundation to disperse various carbon supports. The example shown in Figure 2A indicates the morphology of SWCNT/Pt−Ru deposited on the carbon fiber paper. The carbon nanotubes provide the foundation to anchor Pt−Ru particles. The fine structure of carbon nanotube network can be seen in the magnified view of the image (Figure 2B). Although the carbon nanotubes exist in the form of bundles and ropes, they facilitate dispersion of the catalyst particles and render relatively high active area to the electrode.

Raman spectroscopy has been used to characterize nanotubes and in particular to probe single and multiwalled CNTs. The ring breathing mode (RBM, 120−250 cm^{-1}) and the G band (around 1580 cm^{-1}) are characteristic signatures of single walled nanotubes.[26] The G-band is particularly useful to distinguish between semiconducting and metallic nanotubes. On the other hand, the RBM mode can be used to determine the diameter of the nanotubes and between single and multiwall tubes.[27] In fact multiwall nanotubes do not generally exhibit a peak corresponding to the RBM.

Figures 3A and 3B show the Raman spectrum in the region of 1400−1750 cm^{-1} (G band) and the region of 100−400 cm^{-1} (RBM) for each of the carbon supports deposited on CFE. We have attempted to maintain constant coverage of carbon nanostructures for all the samples. Comparison of the frequencies and line shapes of the G bands (Figure 3A) for the SWCNT samples indicates that both the SES and Bucky USA SWCNT

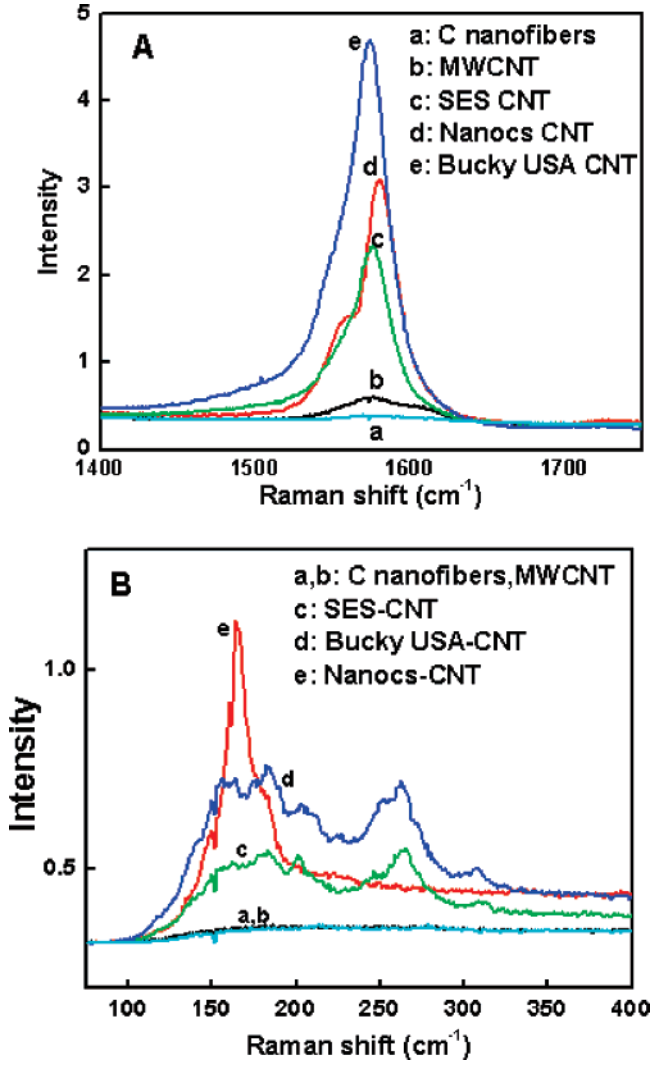

Figure 3. Raman spectra of different samples of carbon supports deposited on a carbon fiber electrode. (A) Raman spectra in the region of the G band: (a) C nanofiber, (b) MWCNT, (c) SES−SWCNT, (d) Nanocs-SWCNT, (e) Bucky USA-SWCNT carbon support. (B) Raman spectra in the region of the RBM band: (a) C nanofiber, (b) MWCNT, (c) SES−SWCNT, (d) Bucky USA-SWCNT, (e) Nanocs CNT carbon support. The spectra shown are an average of two acquisitions and the carbon loading on the sample is estimated to be ∼0.8 mg/cm^2.

samples have substantial metallic character. The presence of a distinct G^- shoulder at lower frequency for the Nanocs sample suggests the presence of smaller diameter tubes that are in resonance with the exciting laser line. The RBM (Figure 3B) also provides useful information on the diameter of the nanotubes. The MWCNTs and nanofibers, as expected, do not show any features in the RBM region, while the Bucky and SES SWCNT samples show a RBM vibration that is considerably broader than that observed for the high surface area Nanocs sample.

Electrochemical Impedance Spectroscopy. Melnick et al.[28,29] have carried out a detailed analysis of the mechanism of methanol oxidation on Pt using impedance spectroscopy. They reported that the rate of charge transfer for the electrooxidation of methanol is a function of potential and coverage of adsorbed intermediate. They conclude that changes in the mechanism for methanol oxidation are caused by the presence of four different species that contain oxygen, each belonging to a specific potential region with the more reactive species at higher potentials.

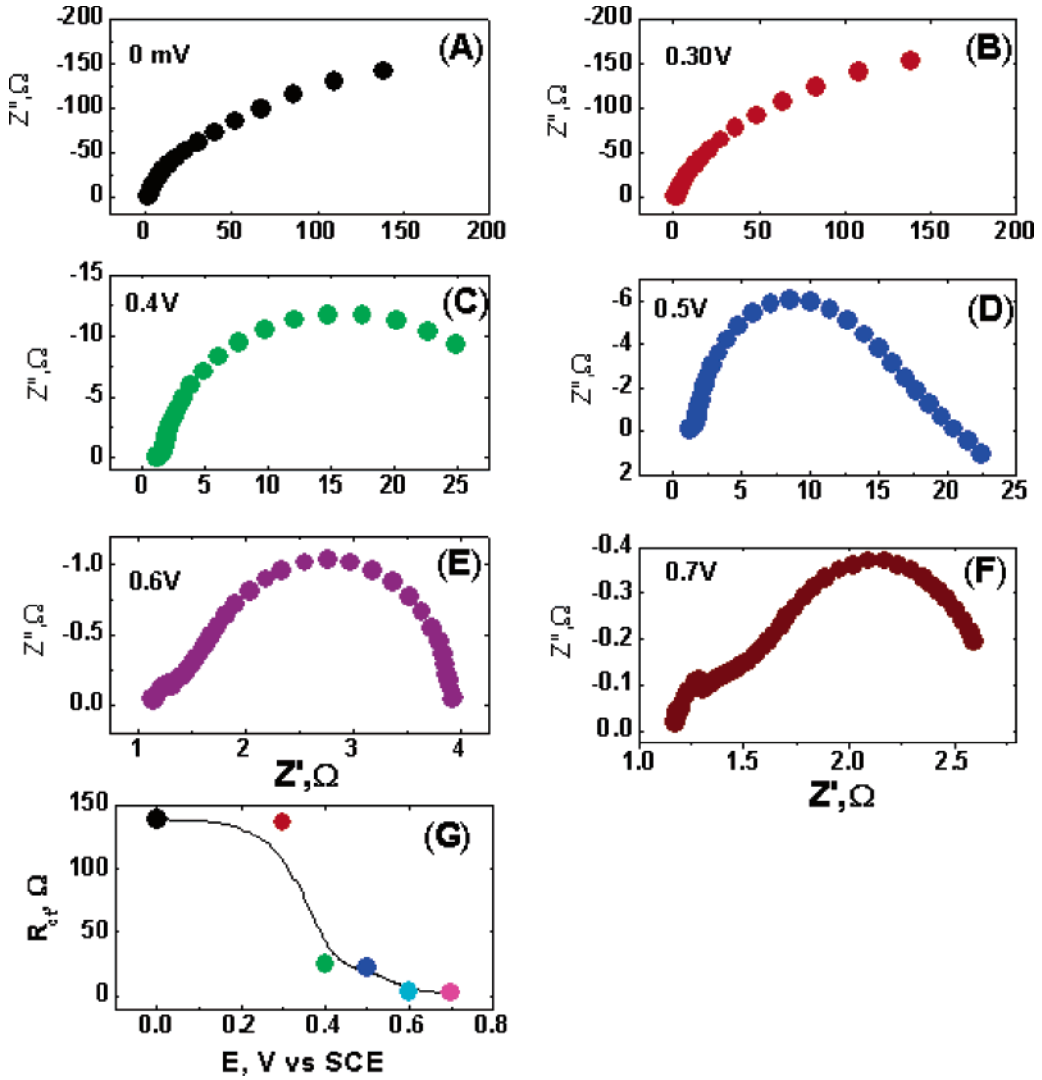

Figure 4. Potential dependent impedance spectra for methanol oxidation in Nyquist form for CFE/SES−SWCNT/Pt−Ru electrode. Figures 4A through F correspond to variation of the potential from equilibrium value: (A) 0 mV, (B) 300, (C) 400, (D) 500, (E) 600, and (F) 700 mV vs SCE. Figure 4G shows the variation of the charge-transfer resistance for the SWCNT electrode with potential. The electrolyte was 1 M methanol in 1 M H_2SO_4. The Pt−Ru loading was 0.2 mg/cm^2 and the amount of carbon support is ∼0.5 mg/cm^2 in each case.

Our study is focused on the impedance response of the electrochemical oxidation of methanol at controlled potentials to understand the role played by carbon nanotubes. As a representative example, we chose SWCNT samples obtained from SES Research. Figures 4 and 5 show the electrochemical impedance spectra for the methanol oxidation reaction at different overpotentials for the CFE/SES−SWCNT/Pt−Ru in the Nyquist and Bode form, respectively. The spectra were obtained in the potential range of 0−800 mV (vs SCE). In the Nyquist form, (Figure 4) the *x*- and the *y*-axes represent the real (Z') and the imaginary (Z'') parts of the impedance spectra, respectively. In the Bode form, (Figure 5A and B) the impedance is plotted with log frequency on the *x*-axis and both the absolute value of the impedance and the phase angle on the *y*-axis. The information on the charge-transfer resistance was obtained by extrapolating the low-frequency region of the semicircle in the Nyquist plots to the real axis.

We have divided the impedance spectra into three regions (Figure 4). Region I corresponds to the potential range between 0 and 300 mV vs SCE, in which double layer charging followed by adsorption of methanol on the electrode surface influences the impedance (Figure 4A and B).[29] The absence of a well-defined semicircle in the Nyquist plot supports such an argument. The Bode plot (traces *a* and *b* in Figure 5A) shows a capacitive behavior for both SWCNT/Pt−Ru and Carbon/Pt−Ru electrodes. This capacitance dependence at low frequency indicates that the SWCNT/Pt−Ru electrode interface is dominated by adsorption and electrical double layer at low overpotential ranges.[30]

Region II (Figure 4C and 4D), which corresponds to the electrode potentials in the range of 400−600 mV, exhibits a well-defined semicircle. These Nyquist plots are indicative of the electrode/electrolyte interface in which the charge-transfer resistance predominates. A plot of charge-transfer resistance (R_{ct}) as calculated from the Nyquist plot with respect to the overpotential for a SWCNT-Pt−Ru electrode is shown in Figure 4G. The charge-transfer resistance for methanol oxidation at Pt−Ru catalysts deposited on a SWCNT support is ∼140 Ω. This value is substantially less than that (∼6 kΩ) of carbon black support (Figure S3 in Supporting Information). In the Bode plots, the capacitance decreases rapidly, indicating the dominance of charge-transfer processes at the electrode/electrolyte interface (traces c and d in Figure 5A). The variation of phase angle with overpotential is shown as an inset of Figure 5B. The phase angle in the case of SWCNT/Pt−Ru electrode decreases from 80 to 10 degrees as the potential varies from 0 to 800

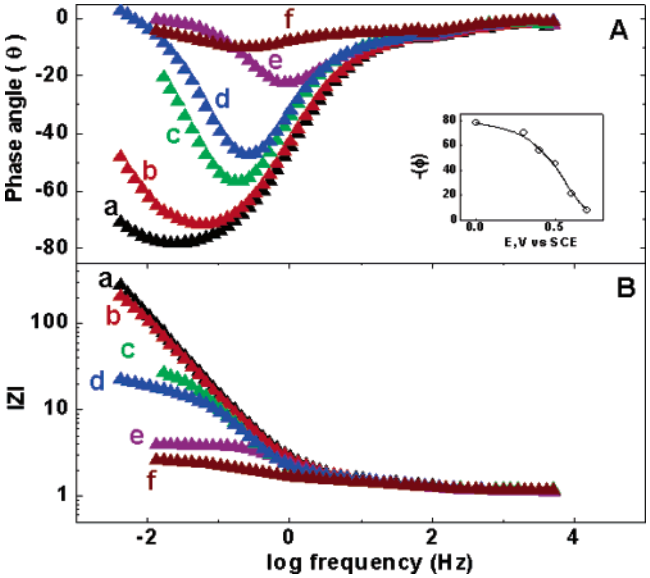

Figure 5. Frequency dependent impedance spectra for methanol oxidation in Bode form for SWCNT/Pt−Ru electrode. Figure 5A shows the dependence of phase angle on the frequency while Figure 5B shows the dependence of the magnitude of impedance on the frequency. In both figures, curves a−f correspond to variation of the potential from equilibrium value: (a) 0 , (b) 300, (c) 400, (d) 500, (e) 600, and (f) 700 mV vs SCE. The inset in Figure 5A shows the variation in phase angle with potential for the SWCNT electrode. The electrolyte was 1 M methanol in 1 M H_2SO_4. The Pt−Ru loading was 0.2 mg/cm^2, and the amount of carbon support is ∼0.5 mg/cm^2 in each case.

mV. In the case of a carbon black support, the high capacitive behavior is retained over the entire potential range as the phase angle changes only from 75 to 40 degrees (see Figure S4 in Supporting Information). The difference in the capacitive behavior of these two electrodes is an indication that the intermediates and charged species are quickly removed from the SWCNT/Pt−Ru electrode surface following methanol oxidation. It further strengthens the argument that the SWCNT support indirectly promotes the methanol oxidation by decreasing the onset potential and charge-transfer resistance.

In region III (Figures 4e and 4f), where the electrochemical potential is in the range of 600−800 mV, the charge-transfer resistance drops by an order of magnitude from 25 Ω to 2.5 Ω. This is accompanied by the complete oxidation of methanol and the removal of the adsorbed intermediates. Since the oxidation of methanol in the high potential range occurs efficiently, we do not observe significant difference between the capacitive behavior of the carbon and SWCNT support based electrocatalysts. Although the role of the carbon support in the methanol oxidation is minimal at high oxidation potentials, the role of carbon nanostructure support becomes more important in the lower oxidation potential region.

Fuel Cell Performance Evaluation of Different Carbon Supports. We have prepared anodes using different carbon supports, the properties of which have been characterized in the previous sections. The typical loading of the electrocatalyst in the anode was Pt−Ru (0.2 mg/cm^2), which was dispersed on SWCNT and other carbon support (∼0.5 mg/cm^2). The cathode in all experiments was fabricated using carbon black (∼2.0 mg/cm^2) and platinum black (1.5 mg/cm^2). Six different membrane electrode assemblies (MEA) were prepared by pressing anodes and the cathode on the opposite side of a pretreated Nafion. The fuel cell testing unit used in the present study is shown in the Supporting Information (Figure S5). The voltage current measurements were done 30 min after methanol

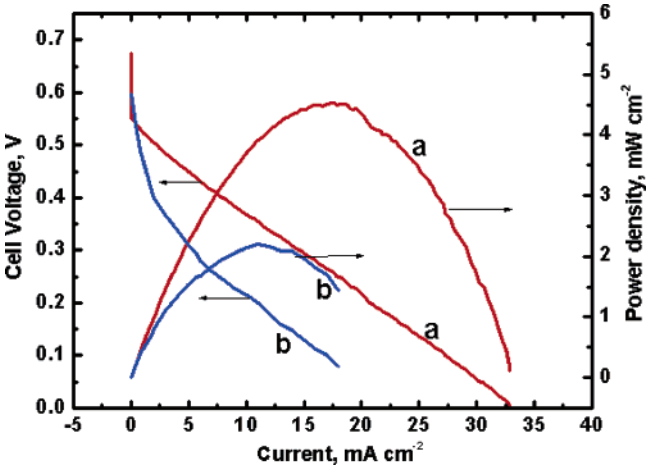

Figure 6. Power density and galvanostatic polarization data at 25 °C of an MEA prepared using (a) CFE/SES−SWCNT/Pt−Ru and (b) CFE/Carbon nanofiber/Pt−Ru anodes. The cathode for both MEAs was Pt black at 1.5 mg/cm^2 dispersed on carbon black (∼2 mg/cm^2). The loading of Pt−Ru on anode electrodes was ∼0.2 mg/cm^2 on ∼0.5 mg/cm^2 of carbon support (SES or C nanofiber). The electrolyte was Nafion 117, electrode area 5 cm^2.

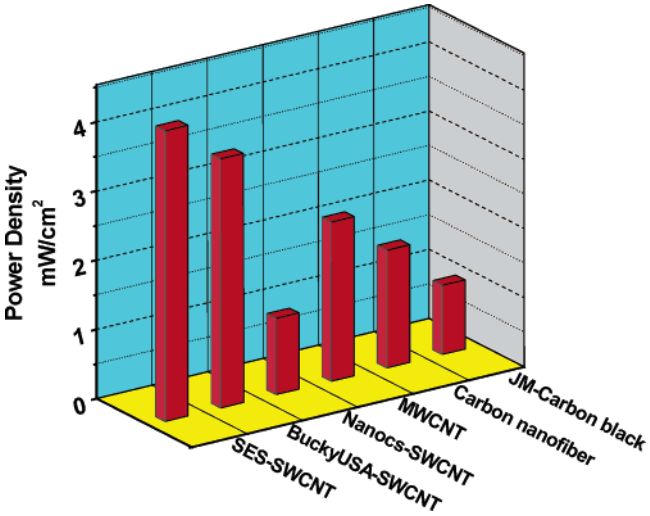

Figure 7. Comparison of power density of passive DMFC cells with different nanostructured carbon supports. The loading of the carbon support at anode was ∼0.5 mg/cm^2 and Pt−Ru catalyst was 0.2 mg/cm^2. The cathode had Pt loading of 1.5 mg/cm^2 and 2.0 mg/cm^2 carbon support. The electrolyte was Nafion 117, electrode area 5 cm^2; temperature 25 °C.

solution was poured into the reservoir, and a potential between 0.6 and 0.7 V was attained. The cell was then subjected to several discharge cycles by holding the potentials at 0.5 and 0.4 V for several minutes so that the MEA was fully functional.

Figure 6 shows the current−potential and power density curves for two different fuel cells using MEA prepared from CFE/SES−SWCNT/Pt−Ru and CFE/carbon nanofiber/Pt−Ru anodes. In the discharge mode, the cell voltage drops rapidly initially in the lower current density region due to limitation of electrode kinetics. As the current density increases, a drop in voltage is observed. The cell resistance and mass transport limitations account for the rapid drop seen at higher current densities. Similar evaluation was also carried out for MEAs prepared by using different carbon supports. We compare the maximum power densities obtained with these MEAs in Figure 7. The MEAs fabricated using the SWCNT samples from SES and Bucky USA gave the best performance, with a power density of ∼4 mW/cm^2. The power density values obtained in

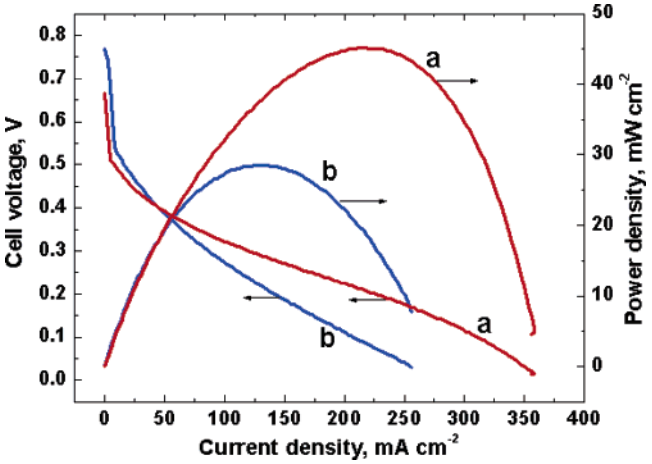

Figure 8. DMFC fuel cell polarization data and the power density curves for (a) MEA using CFE/SES−SWCNT/Pt−Ru anode and CFE/SES−SWCNT/Pt cathode. (b) MEA using CFE/Carbon black/Pt−Ru anode and CFE/Carbon black/Pt cathode. The loading of SWCNT or carbon black at the anode was 1.0 mg/cm^2 and at the cathode was 2.0 mg/cm^2. The Pt−Ru catalyst loading at the anode was 0.8 mg/cm^2 and Pt catalyst loading at cathode was 1.5 mg/cm^2. The membrane was Nafion 117 and the cell was operated at 70 °C. 1 M Methanol was flowed through anode at a flow rate of 0.005 L/min, and oxygen was flowed through cathode at a flow rate of 0.5 L/min.

these experiments are similar to those observed for a small portable DMFC.[31,32] Even MWCNTs and carbon fiber supports employed in MEA exhibited reasonably good power density of ~2 mW/cm^2. Overall, these carbon nanotube supports exhibit a better performance toward enhancing the electrocatalytic activity of Pt−Ru catalysts.

Given that the SES nanotube samples exhibit the best fuel cell performance at room temperature in comparison with the other supports, we further extended its performance evaluation in a single cell at higher temperatures. Both anode and cathode of the PEM consisted of SWCNT support. In contrast with the air breathing cell, the methanol was circulated through the anode compartment and O_2 was passed through the cathode. Since methanol oxidation proceeds more efficiently at higher temperature, we expect to see enhanced power densities at 70 °C. Figure 8 shows the polarization curves at 70 °C for an MEA with a CFE/SES−SWCNT/Pt−Ru anode and CFE/SES−SWCNT/Pt cathode. For comparison we have also evaluated a MEA using carbon black at both anode and cathode. The loading of SWCNT and other carbon support at the anode was 1.0 mg/cm^2 and at the cathode was ~2.0 mg/cm^2. The catalyst loading at the anode was Pt−Ru 0.8 mg/cm^2 and cathode Pt metal loading was maintained at 1.5 mg/cm^2. At 70 °C we observe a power density value of 45 mW/cm^2 for SWCNT/Pt−Ru anode. This value is greater than the value obtained for the carbon/Pt−Ru anode (28 mW/cm^2). More than 30% improvement in the power density can thus be achieved by employing carbon nanotubes as support material. Such an increase is consistent with the catalytic enhancement and effective utilization of the Pt−Ru on SWCNT based carbon support in DMFC.

The results presented here show the importance of carbon nanostructures as support materials to disperse Pt−Ru catalyst particles quite effectively. As evident from Table 1, Pt−Ru catalysts dispersed on single wall carbon nanotubes exhibit lower onset potential for methanol oxidation. The onset potential for methanol oxidation correlates well with the maximum power density of DMFC. Based on the evaluation of the electrochemical and fuel cell performances, we can conclude that no single property of the carbon nanostructures dictate the performance of electrocatalysts in the MEA. Along with the electrochemically active surface area of the MEA, intrinsic properties such as metallic characteristics of nanotubes are important in attaining higher power density of DMFC. The carbon nanotubes obtained from SES Research and Bucky USA with similar ECSA and metallic character show the best performance. Nearly 30% enhancement in the power density is seen when these carbon nanotubes are used in the MEA instead of carbon black. The shift in the onset potential for methanol oxidation and lower charge transfer resistance are further indication that these carbon nanotubes are catalytically active in promoting methanol oxidation at Pt−Ru electrocatalyst.

Acknowledgment. The research described herein was supported by the Indiana 21st Century Research and Technology Fund and the U.S. Army CECOM RDEC through Agreement DAAB07-03-3-K414. Such support does not constitute endorsement by the U.S. Army of the views expressed in this publication. This is contribution no. NDRL 4625 from Notre Dame Radiation Laboratory.

Supporting Information Available: Figures S1-S5 are available free of charge via the Internet at http://pubs.acs.org.

References and Notes

(1) Dyer, C. K. *J. Power Sources* **2002**, *106*, 31.
(2) Dillon, R.; Srinivasan, S.; Arico, A. S.; Antonucci, V. *J. Power Sources* **2004**, *127*, 112.
(3) Schultz, T.; Zhou, S.; Sundmacher, K. *Chem. Eng. Technol.* **2001**, *24*, 1223.
(4) Gogel, V.; Frey, T.; Yongsheng, Z.; Friedrich, K. A.; Jorissen, L.; Garche, J. *J. Power Sources* **2004**, *127*, 172.
(5) Kinoshita, K. *Carbon: Electrochemical and Physicochemical Properties*, 1st ed.; Wiley-Interscience: New York, 1988.
(6) Serp, P.; Corrias, M.; Kalck, P. *Appl. Catal. A* **2003**, *253*, 337.
(7) Che, G. L.; Lakshmi, B. B.; Fisher, E. R.; Martin, C. R. *Nature* **1998**, *393*, 346.
(8) Rajesh, B.; Thampi, K. R.; Bonard, J. M.; Xanthopoulos, N.; Mathieu, H. J.; Viswanathan, B. *J. Phys. Chem. B* **2003**, *107*, 2701.
(9) Mastragostino, M.; Missiroli, A.; Soavi, F. *J. Electrochem. Soc.* **2004**, *151*, A1919.
(10) Bessel, C. A.; Laubernds, K.; Rodriguez, N. M.; Baker, R. T. K. *J. Phys. Chem. B* **2001**, *105*, 1115.
(11) Steigerwalt, E. S.; Deluga, G. A.; Lukehart, C. M. *J. Phys. Chem. B* **2002**, *106*, 760.
(12) Che, G. L.; Lakshmi, B. B.; Martin, C. R.; Fisher, E. R. *Langmuir* **1999**, *15*, 750.
(13) Li, W. Z.; Liang, C. H.; Qiu, J. S.; Zhou, W. J.; Han, H. M.; Wei, Z. B.; Sun, G. Q.; Xin, Q. *Carbon* **2002**, *40*, 791.
(14) Carmo, M.; Paganin, V. A.; Rosolen, J. M.; Gonzalez, E. R. *J. Power Sources* **2005**, *142*, 169.
(15) Girishkumar, G.; Vinodgopal, K.; Kamat, P. V. *J. Phys. Chem. B* **2004**, *108*, 19960.
(16) Li, X. G.; Ge, S. H.; Hui, C. L.; Hsing, I. M. *Electrochem. Solid State Lett.* **2004**, *7*, A286.
(17) Li, W. Z.; Liang, C. H.; Zhou, W. J.; Qiu, J. S.; Li, H. Q.; Sun, G. Q.; Xin, Q. *Carbon* **2004**, *42*, 436.
(18) Girishkumar, G.; Rettker, M.; Underhile, R.; Binz, D.; Vinodgopal, K.; McGinn, P.; Kamat, P. V. *Langmuir* **2005**, *21*, 8487.
(19) Watanabe, M.; Motoo, S. *J. Electroanal. Chem.* **1975**, *60*, 267.
(20) Watanabe, M.; Zhu, Y. M.; Igarashi, H.; Uchida, H. *Electrochemistry* **2000**, *68*, 244.
(21) Liu, Z. L.; Ling, X. Y.; Su, X. D.; Lee, J. Y. *J. Phys. Chem. B* **2004**, *108*, 8234.
(22) Suzuki, S.; Bower, C.; Watanabe, Y.; Zhou, O. *Appl. Phys. Lett.* **2000**, *76*, 4007.
(23) Choi, H. C.; Shim, M.; Bangsaruntip, S.; Dai, H. J. *J. Am. Chem. Soc.*, **2002**, *124*, 9058.
(24) Gasteiger, H. A.; Kocha, S. S.; Sompalli, B.; Wagner, F. T. *Appl. Catal. B* **2005**, *56*, 9.
(25) Ralph, T. R.; Hards, G. A.; Keating, J. E.; Campbell, S. A.; Wilkinson, D. P.; Davis, M.; St. Pierre, J.; Johnson, M. C. *J. Electrochem. Soc.* **1997**, *144*, 3845.
(26) Jorio, A.; Pimenta, M. A.; Souza, A. G.; Saito, R.; Dresselhaus, G.; Dresselhaus, M. S. *New J. Phys.* **2003**, *5*.

(27) Dresselhaus, M. S.; Dresselhaus, G.; Jorio, A.; Souza, A. G.; Pimenta, M. A.; Saito, R. *Acc. Chem. Res.* **2002**, *35*, 1070.
(28) Melnick, R. E.; Palmore, G. T. R. *J. Phys. Chem. B* **2001**, *105*, 9449.
(29) Melnick, R. E.; Palmore, G. T. R. *J. Phys. Chem. B* **2001**, *105*, 1012.
(30) Sugimoto, W.; Aoyama, K.; Kawaguchi, T.; Murakami, Y.; Takasu, Y. *J. Electroanal. Chem.* **2005**, *576*, 215.
(31) Blum, A.; Duvdevani, T.; Philosoph, M.; Rudoy, N.; Peled, E. *J. Power Sources* **2003**, *117*, 22.
(32) Shimizu, T.; Momma, T.; Mohamedi, M.; Osaka, T.; Sarangapani, S. *J. Power Sources* **2004**, *137*, 277.